Supporting Information

Structure optimization of perovskite quantum dot light-emitting diodes

Qasim Khan,[a] Alagesan Subramanian,[b] Guannan Yu,[a] Khan Maaz,[b] Delong Li,[a] Rizwan Ur Rehman Sagar,[c] Keqiang Chen,[a] Wei Lei,[b] Babar Shabbir,[d] Yupeng Zhang,[a*]

[a]*Shenzhen Key Laboratory of Flexible Memory Materials and Devices, College of Electronic Science and Technology, Shenzhen University, Shenzhen 518000, China.*

[b]*Joint International Research Laboratory of Information Display and Visualization, School of Electronic Science and Engineering, Southeast University, Nanjing, Jiangsu 210096, China.*

[c]*Graduate School at Shenzhen, Tsinghua University, Shenzhen, 518055, China*

[d]*Department of Materials Science and Engineering and ARC Centre of Excellence in Future Low-Energy Electronics Technologies (FLEET), Monash University, Clayton, Victoria 3800, Australia*

*Corresponding author: ypzhang@szu.edu.cn (Y. Z).

Isolation of $CsPbBr_3$ quantum dots. The as-synthesized $CsPbBr_3$ quantum dots (QDs) were precipitated by adding 200 ml MeOAc (the ratio of reaction solution:MeOAc is 1:3) and centrifuged at 8000 rpm for 5 min. The pellet in the centrifuge tube was dispersed in 3 ml hexane and 3ml MeOAc, and then centrifuged at 8000 rpm for 2 min. The $CsPbBr_3$ QDs were dispersed again in 20 ml hexane and centrifuged at 4000 rpm for 5 min to remove excess Cs-oleate and

PbI_2. The $CsPbBr_3$ QDs were kept under dark at 4 ^oC for 48 h. For device fabrication, $CsPbBr_3$ QDs were dissolved in toluene at a concentration of 15 mg ml^{-1}.

TEM images of the TNPs and LiTNPs.

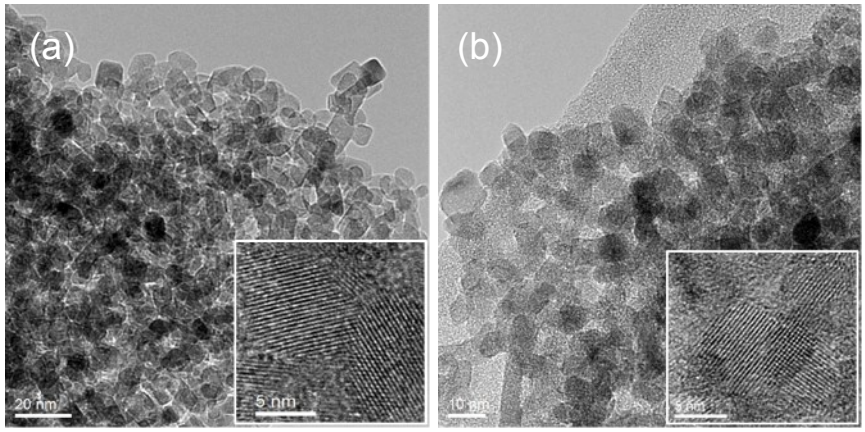

Figure S1 (a) TEM with its corresponding HRTEM images (Inset) of LiTNPs and (b) TNPs.

XPS spectra of the TNPs and LiTNPs.

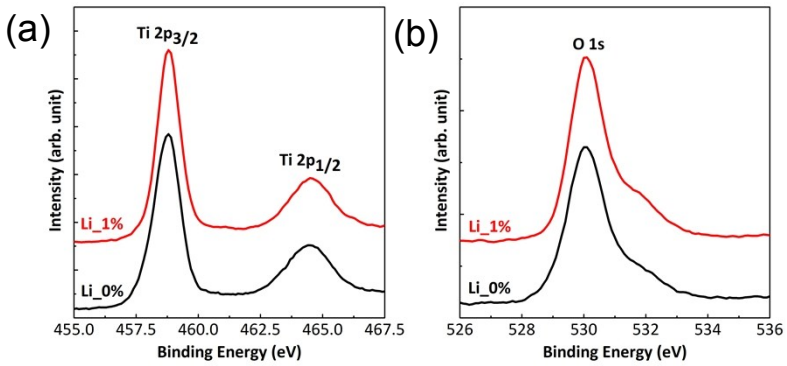

Figure S2 XPS spectra of TiO_2 and Li-doped TiO_2 nanoparticles in (a) Li 1s region and (b) O 1s region.

XPS Spectra of $CsPbBr_3$ QDs

The chemical composition and the detailed chemical bonding status of the $CsPbBr_3$ are analyzed using XPS measurement (Figure 4). The peaks for Cs $3d_{5/2}$, Cs $3d_{3/2}$ in the Cs 3d spectrum are observed at 725.20 eV and 739.15 eV, respectively. In the Pb 4f spectrum, peaks at 138.80 eV, 143.65 eV indicate the existence of Pb $4f_{7/2}$ and Pb $4f_{5/2}$. The peaks at 68.3 eV, 69.4 eV belongs to Br $3d_{5/2}$ and Br $3d_{3/2}$ in the Br 3d spectrum.[1, 2]

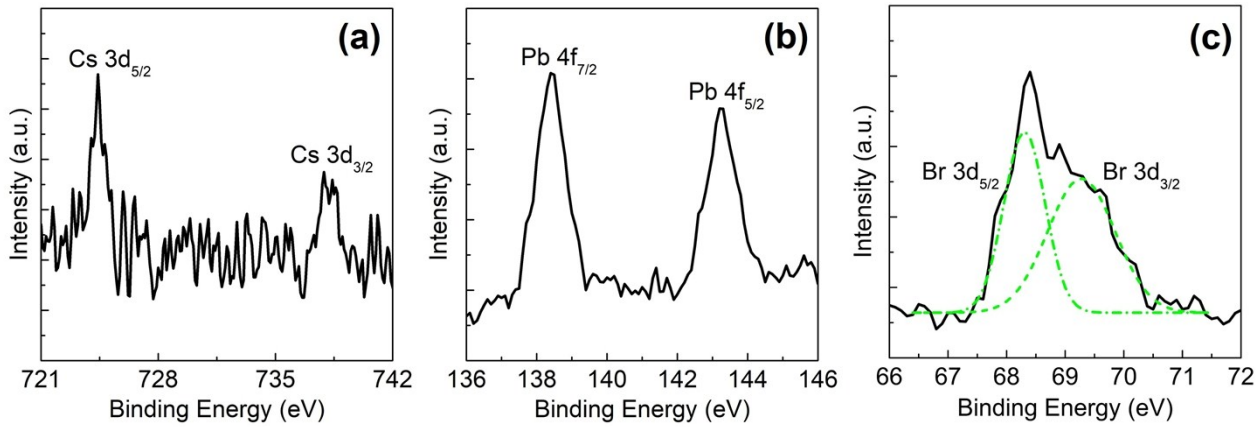

Figure S3 (a) Cs 3d, (b) Pb 4f, and (c) Br 3d XPS spectra of the $CsPbBr_3$ QDs.

Calculation of photoluminance quantum yield of the $CsPbBr_3$ QDs

The quantum yield (Φ) of the $CsPbBr_3$ QDs was calculated using rhodamine 6G, which has a known QY of 0.95, as the standard. The Φ was calculated by the following equation [3]

$$\Phi_X = \Phi_S \left(\frac{I_X}{I_S}\right)\left(\frac{\eta_X^2}{\eta_S^2}\right)\left(\frac{A_S}{A_X}\right)$$

Where Φ, I, η and A are the quantum yield, integrated emission intensity, refractive index of the solvent and optical density of the standard rhodamine 6G (S) and the $CsPbBr_3$ QDs (X). The calculated Φ value of the as-synthesized $CsPbBr_3$ QDs is 78%.

In order to accurately measure the absolute photoluminescence quantum yield (PLQY) of the CsPbBr3 QDs thin films, we have adopted an integrated monochromatic excitation light source integrating sphere-based detection system without using any reference sample. The excitation power density was kept constant (at 50 mW/cm^2) for all these samples deposited on a cleaned quartz substrate. The films PLQY were calculated and found to be 36%. The PLQY of this film is slightly decreased to 34.5% when methanol was spin coated as like TNPs thin film is deposited, is due to the anti-solvent degradation effect.

TEM images of the $CsPbBr_3$

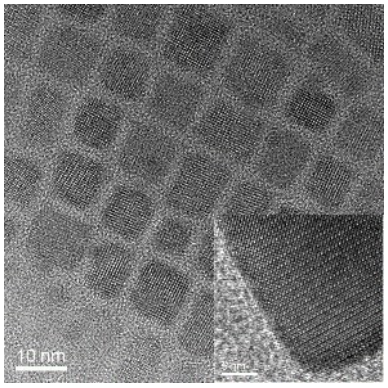

Figure S4 TEM and the corresponding HR-TEM (inset) images of the $CsPbBr_3$ QDs.

ETL thickness optimization and characterization

In order to optimize the TNPs/LiTNPs layer thickness, we fabricated inverted QLED devices and measured their EL as shown in the Figure S5(a). We found the optimized thickness of the oxide based

ETL is 90 nm. As can be seen, for the thinner (<90 nm) the luminance was significantly lower as well as for the thicker (>90 nm) the brightness started to decrease. This might be due to the well-balanced carriers injection into the QDs layer by the 90 nm thick ETL.

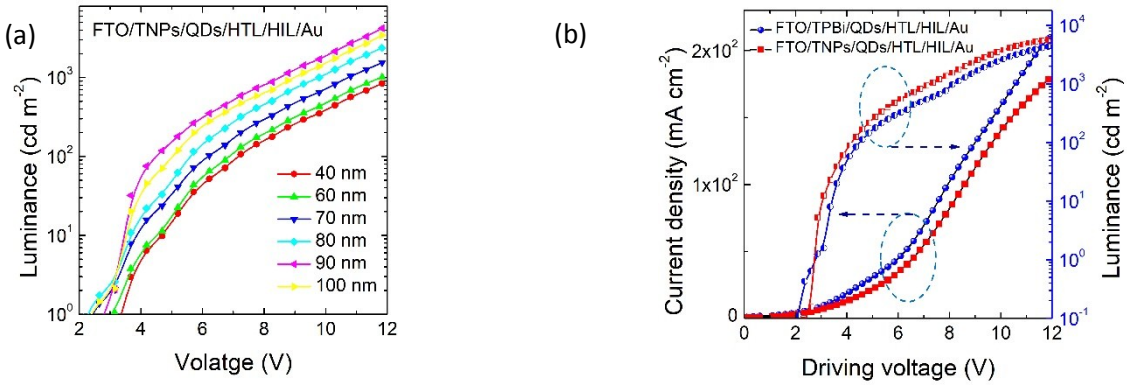

Figure S5 (a) Luminance versus voltage characteristics of the QLEDs based on varied ETL thickness. (b) Current density and luminance versus driving voltage characteristics of the controlled devices.

Besides, we fabricated control devices in the inverted structure having 45 nm TPBi and 90 nm thick TNPs electron transporting layers. The luminance and current density versus driving voltage was measured as shown in the Figure S5(b). The TNPs based QLED device has higher luminance and lower current density than the TPBi based QLED device. The higher luminance is the result of the better carriers recombination inside the QDs layer due to the better hole blockage by the TNPs ETL. Whereas the TPBi based device has higher current density which is most probably due to the higher leakage current caused by the low-lying HOMO level of the TPBi and hence the injected hole are not efficiently confined inside the QDs layer. This lower confinement of holes into the QDs layer causing the higher current density and lower luminance. In addition, the TPBi layer consisting device have rather lower operating voltages (<2.5 V) which is might be due to the charge accumulation assisted Auger recombination at either of the interfaces.

PL quenching analysis

In order to explain the charge interaction between the ETL and QDs layer, we performed a series of experiments to investigate the energy transfer analysis between these layers, TNPs and LiTNPs films were deposited on HTL/QDs films. These semi-devices (Poly-TPD/$CsPbBr_3$/TNPs and Poly-TPD/$CsPbBr_3$/LiTNPs) under excitation with the 380 nm source, exhibited similar photoluminescence (PL) emissions but different intensities, as shown in Figure S6. Specifically, the PL intensity of the device with the TNPs layer was decreased by 20% in comparison with the device having the LiTNPs layer. The electron-hole dissociation takes place and the generated electrons are efficiently transferred to TNPs layer due to the larger energy offset compared to the LiTNPs layer. Hence, the TNPs layer is more favorable for the exciton quenching resulting into the decreased PL.

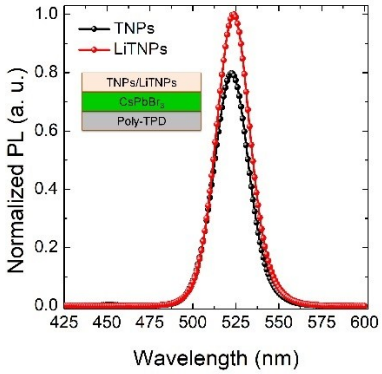

Figure S6 Photoluminance quenching of the poly-TPD/QDs/ETLs devices.

Mobility measurement of the ETL

In order to study the effect of annealing temperature on the mobility of TiO_2 NPs, thin-film transistors (TFTs) were fabricated using TNPs/LiTNPs as the channel materials at constant annealing time of 30 minutes. The charge-carrier mobility in the TFTs was extracted from their transfer characteristics (see Figure) using the following relationship between the saturated drain current I_{Dsat} and the gate voltage V_G:

$$I_{Dsat} = \frac{W}{2L}\mu C(V_G - V_T)^2 \quad (1)$$

where L is the channel length, W is the channel width, μ is the mobility, C is the gate capacitance per unit area, and V_T is the threshold voltage. The electron mobility was observed to continuously increase with an increasing annealing temperature of these NPs. The carrier mobility in undoped TNPs when annealed at 100℃ was found to be 1.6×10^{-4} cm^2 V^{-1} s^{-1} which is comparable to previously reported values.[4] The carrier mobility further increased as the annealing temperature increased to 150℃ achieved the value of μ_{emax} = 2.8×10^{-4} cm^2 V^{-1} s^{-1}. Similar trend has been observed for the Li doped TNPs when annealed at different temperatures. LiTNPs thin films had electron mobilities of 4.1×10^{-3} and 5.7×10^{-3} when annealed at 100℃ and 150℃, respectively. As a result of this enhanced electron mobility, the conductivity of these thin films also increased with increasing annealing temperature (Table 1). Electrical characterization of these TFTs was performed using a semiconductor parameter analyzer (HP 4155C) in a nitrogen atmosphere where gate voltage was varied at the rate of 0.1 V at the constant source-drain voltage of 30 V.

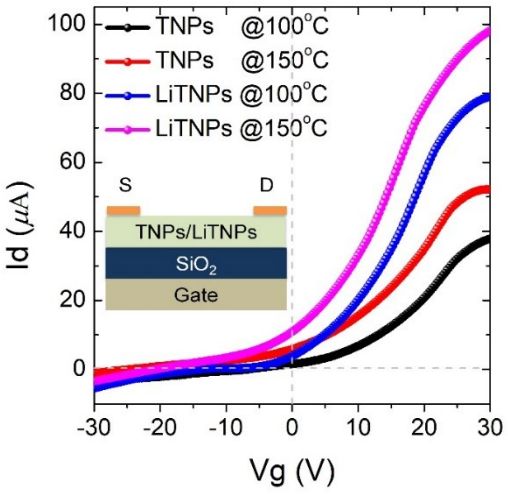

Figure S7 Field-effect transistor (FET) characteristics of the TNPs/LiTNPs films fabricated on a Si/SiO_2 substrate. Inset: Schematic diagram of the TFT structure.

Table 1. Electrical properties of TiO_2 and Li-TiO_2 nanoparticles.

Parameters	TNPs @100^{o}C	TNPs @150^{o}C	LiTNPs @100^{o}C	LiTNPs @150^{o}C
Sheet resistance (Ω.cm)	7.35 ±0.01	7.27 ±0.1	7.22 ±0.15	7.12 ±0.02
Conductivity σ (Ω.cm^2)	6.22 ±0.6	-----	8.81 ±0.5	-----
Mobility μ (cm^{2}V^{-1}s^{-1})	1.6×10^{-4} ±0.02	2.8×10^{-4} ±0.01	4.1×10^{-3} ±0.05	5.7×10^{-3} ±0.05
Contact resistance ($\mu\Omega$)	486 ±5	370 ±1	245 ±5	133 ±3

REFERENCES

1. Cho, H., et al., *High-Efficiency Solution-Processed Inorganic Metal Halide Perovskite Light-Emitting Diodes.* Adv Mater, 2017. **29**(31).
2. Le, Q.V., et al., *Investigation of Energy Levels and Crystal Structures of Cesium Lead Halides and Their Application in Full-Color Light-Emitting Diodes.* Advanced Electronic Materials, 2017. **3**(1).
3. Lin, L.X. and S.W. Zhang, *Creating high yield water soluble luminescent graphene quantum dots via exfoliating and disintegrating carbon nanotubes and graphite flakes.* Chemical Communications, 2012. **48**(82): p. 10177-10179.
4. Chen, H.-Y., et al., *Polymer solar cells with enhanced open-circuit voltage and efficiency.* Nature photonics, 2009. **3**(11): p. 649.